

Very Early Formation of Big, Liquid Drops Revealed by Z_{DR} in Continental Cumulus

CHARLES A. KNIGHT

National Center for Atmospheric Research, Boulder, Colorado*

(Manuscript received 6 July 2004, in final form 30 November 2005)

ABSTRACT

Examination of the early radar echo histories of several vigorous, cumulus clouds in northeast Colorado and northwest Kansas, with sensitive, dual-polarization radar, reveals the formation of millimeter-sized water drops at about the same time that the conventional, first precipitation echo (from ice) forms aloft. The early, positive Z_{DR} values appear in the vicinity of the 0°C level (the radar data do not specify height accurately) and soon extend both above and below it. Positive Z_{DR} is found within and to the upwind side of the updraft, separate from the conventional first precipitation echoes, which appear first at higher altitude, generally downwind of the updraft core, and have no significantly positive Z_{DR} . Big, liquid drops were not expected this early in the formation of continental cumulus. The early presence of supercooled water drops larger than cloud droplets may be a significant factor in the glaciation of these clouds.

The kind of early radar coverage illustrated here would be a priceless adjunct to aircraft studies of precipitation formation in cumulus. Microphysical data from aircraft must be interpreted with numerical models in order to deduce (or verify) the processes, and such models require the kind of early data illustrated here, both for initialization and verification.

1. Introduction

The growth of precipitation in cumulus clouds may be viewed as two stages: the initial growth of significant quantities of hydrometeors large enough to have appreciable fall velocities (greater than around 0.5 m s^{-1} , say), and a later stage in which such particles are already present. While the distinction is vague because the words significant and appreciable are not specific, it can be useful for reasoning about clouds because the important processes in the two stages may differ. In the first stage we think of primary processes such as droplet activation followed by condensation growth, then followed either by coalescence growth of liquid drops or by ice nucleation with subsequent vapor growth and riming. In the later stage, secondary processes such as drop breakup and Hallett–Mossop ice multiplication may dominate the creation of new, precipitation-sized hydrometeors.

The time for the secondary processes to dominate—if they do come to dominate—is important because many cumulus clouds do not last long. For them it is likely to be a major factor in determining how much precipitation is produced. An analysis of cumulus cloud-seeding results in Montana (Cooper and Lawson 1984) provides a good example of this. A major goal of cloud physics research is to understand the primary processes of hydrometeor growth well enough to predict the first stage of precipitation formation with confidence, either as defined above or however it might be defined more specifically. Since the mature stages of rain clouds and thunderstorms generally involve a combination of primary and secondary processes that is difficult to unravel, it makes sense to study the primary processes early enough in a cloud's evolution that the secondary ones have not yet had time to get started.

This is hard to accomplish in cumulus using aircraft, because it is difficult to recognize a cloud in which precipitation will form early enough to get an aircraft into it in time. Also, important concentrations of the hydrometeors at the large end of the size spectrum may be too low to be sampled adequately. Detailed study of radar first echoes may be more useful for studying the first stage of precipitation formation, using sensitive, modern radars: especially since the advent of polariza-

* The National Center for Atmospheric Research is sponsored by the National Science Foundation.

Corresponding author address: Dr. Charles A. Knight, National Center for Atmospheric Research, P.O. Box 3000, Boulder, CO 80307-3000.

E-mail: knightc@ucar.edu

tion techniques, which have decreased the ambiguities of interpretation (e.g., Vivekanandan et al. 1999).

The present investigation is an exploratory study of the early radar echo development in cumulus clouds in an area encompassing the northern part of the Colorado–Kansas border, carried out in Severe Thunderstorm Electrification and Precipitation Study (STEPS) during May–July 2000 (Lang et al. 2004). Data from the S-Pol and CHILL radars, both 10-cm wavelength with dual polarization, are used for the purpose of seeing what they can reveal about the microphysical processes involved in the first formation of precipitation in cumulus. Using Z_{DR} , it had been found that large drops develop surprisingly early and surprisingly low in cumulus in Florida (Knight et al. 2002). Since the clouds in the STEPS area are more continental and have colder bases, there was no strong expectation that there would be any significantly positive Z_{DR} in their early echoes. If the first precipitation development was by the ice process and the first echoes were from low concentrations of graupel, one might expect Z_{DR} values close to zero throughout the early formation of precipitation. The main result here is that big drops (positive Z_{DR}) are sometimes present very early in these clouds too.

A second objective in this study, which is perhaps more important in the long run, was to try to determine meaningful times for first precipitation echoes. Before the primary ice process can produce significant amounts of precipitation, a low enough temperature must be reached for enough ice crystals to nucleate. In general one expects that temperature to be no warmer than about -10°C , and the time might be measured from the time that cloud top rises past that or some other temperature level. This kind of information has not been available, though it is fundamentally important and radar can be used to obtain it. Cloud tops are usually visible by Bragg scattering with modern, sensitive, C- or S-band radar (5- or 10-cm wavelength) and the precipitation echo may be distinguished from Bragg scattering by its location, stronger intensity, and rate of intensification (Knight and Miller 1998). If information on early cloud-top heights along with the early echo histories were available, the time it takes to produce observed echo intensities could be compared in a very general way to calculations from expectations of ice nucleus concentrations and rates of graupel formation via the ice process, to see if there are any large, unexplained discrepancies.

A serious problem, which will be mentioned in the concluding discussion, is how best to scan the radar to get useful, early data on cumulus that will then grow to much larger size.

2. Results

The first step in the analysis was to examine all the STEPS S-Pol data systematically, seeking early echo cases with complete enough coverage to be included. Data from the CHILL radar were examined only from the 29 June and 5 July cases. The first, second, and fourth cases presented below were obtained during the coordinated scanning of mature storms. That scanning comprised 2 PPI volume scans (scanning in azimuth at several fixed elevations; PPI stands for plan position indicator) and 1 or 2 RHI volume scans (scanning in elevation at several fixed azimuths; RHI stands for range–height indicator) and one survey scan at 0.5° elevation every 13 min. The RHI volume scans typically covered about 10° azimuth centered on the high reflectivity part of a mature storm, while the PPI volumes covered a much wider sector, usually more than 50° . The first case described below was the only one that happened to be included in the RHI sector. Luckily, its azimuth was also such that the RHI planes were about parallel to the wind shear and the cloud motion, so data from the RHIs illustrate its radar history very well. The second and fourth cases were covered only in the PPI volumes, giving about 6.5-min time resolution. The third case, 4 July, was covered in survey mode only, with six 360° scans from 0.5° to 5.5° elevation every 6 min, but it also was well oriented for RHIs. It was recognized as a good case, though at very long range, and a single RHI volume was taken.

In three of the four cases presented here, there are values of Z_{DR} that are interpreted as indicating raindrops, at low values of Z_e , at about the same time that the conventional first precipitation echo appears. (Conventional first precipitation echoes are those that would normally be identified as precipitation without the aid of Z_{DR} . In the cases presented below they are composed of ice, occur above the freezing level, have essentially zero Z_{DR} , and intensify rapidly.) The early, positive Z_{DR} values are separate from them, appearing within or upwind of the presumptive updraft, while the conventional first echoes are downwind. The following subsections contain descriptions of these cases.

a. 29 June

The case on 29 June is both the most complete and the most energetic one, with the cloud top rising above 15-km MSL. It might be worth more detailed study, including multiple Doppler analysis of its wind fields, though the time and space resolution of the data are not what one might wish. Here the purpose is description and illustration as one example of the early echo behavior. The Z_{DR} history is emphasized as the most novel and interesting aspect.

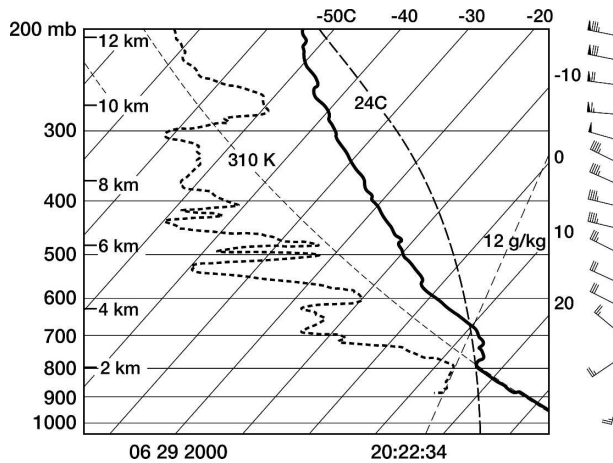


FIG. 1. Sounding for the 29 June case, from Tessendorf et al. (2005). Ascent along the 24°C pseudoadiabat was assumed, after several hours' surface heating. Heights in km MSL. Full wind barb is 10 m s⁻¹.

The cell grew east of the radar, starting above a radar “thin line” (Wilson et al. 1994), a more or less linear accumulation of insects in the boundary layer that indicates low-level convergence. (The S-Pol data alone did not show convergence, since the radar was looking directly down the line, but multiple-Doppler analysis done for the severe storm did reveal convergence along the south side of the line (L. J. Miller 2003, personal communication). The thin line echoes are not always very thin, but are characterized by high values of Z_{DR} and LDR along with equivalent reflectivity factors often as high as 15 dBZ, occasionally higher. Convective initiation is often associated with them (Wilson and Schreiber 1986) but they commonly occur without such initiation, and are only sometimes useful predictors.

Figure 1 is the sounding deemed most representative of the low-level conditions appropriate for this case, which is also the sounding used for the main storm (Tessendorf et al. 2005). It was taken at Goodland at 2022:34 (all times herein are UTC) and had a convective available potential energy (CAPE) of 1254 J kg⁻¹. The low-level temperatures were increased about 3°C (not shown in Fig. 1) for the analysis of cloud-base conditions because of the time difference between the sounding and the storm, and the low-level winds were altered using radar data.

Figure 2 shows the time–height history of maximum Z_e , with an outline of the area containing significant values of positive Z_{DR} related to hydrometeors in the cloud. There is no attempt to contour maximum Z_{DR} values because the data are usually noisy within 1 or 2 dB, and the whole range is only about 4 dB. (For examples, see especially the Z_{DR} panels of Figs. 3c and 3d and Figs. 7e and 8, below). The × symbols are used to

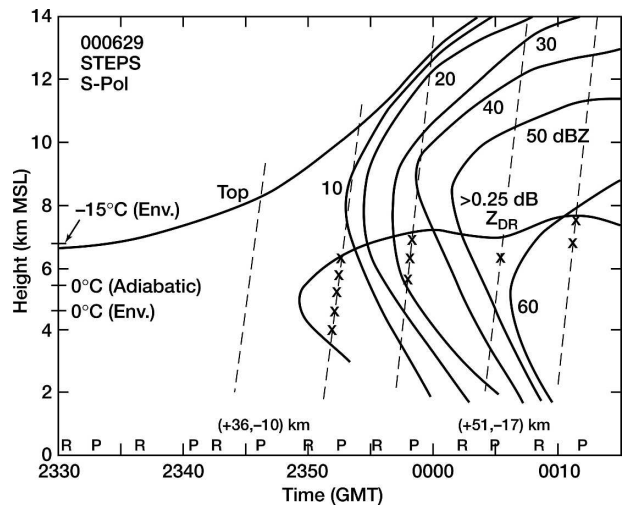


FIG. 2. Time–height diagram of maximum Z_e for the 29 June case, with the envelope of Z_{DR} values above 0.25 dB superimposed. The slanting dashed lines represent the PPI sweeps, with the × symbols indicating those close to the boundary of the area in which significant Z_{DR} values >0.25 dB existed. The RHI and PPI scan times are indicated by “R” and “P” symbols along the abscissa, as are the locations of the cloud at two times, in radar coordinates. The environmental and in-cloud 0°C levels are indicated, as well as the environmental −15°C level.

locate the positions of significant, positive Z_{DR} signals that define the boundary of the area within which they occur. Once rain reaches the ground as indicated by the Z_e value, the positive Z_{DR} always reaches the ground too, with values of 3dB and higher (see Figs. 3e and f).

Figure 3 shows the evolution of the radar structure. The layer of insect echo is sharply defined in the Z_{DR} panels of Figs. 3a and 3b, where the gray signifies Z_{DR} above 4.25 dB, the top of the color table. The top of this layer is at about 3 to 3.5 km MSL and is strikingly sharp and flat, viewed with Z_{DR} , at these two times. In Figs. 3c and 3d, lower values of Z_{DR} descend into this layer from the top, and where this is happening the linear depolarization ratio (LDR) is extremely high: −6 dB and above. (If the scatterers were spheres, LDR would be 0, or −∞ dB. LDR values in precipitation are normally below −20 dB, as seen in the LDR panels of Figs. 3e and 3f. Thus −6 dB is very high.) These features are connected somehow with the growing, convective cloud, and similar features occur in other cases, but their origin is not understood. They are not closely correlated with any other radar features that suggest precipitation, yet one must imagine that they have something to do with it. Substantial precipitation is reaching the ground in Figs. 3e and 3f, and where that occurs the precipitation echo masks that from the insects. The insect layer extends right to the wall of precipitation in Fig. 3f.

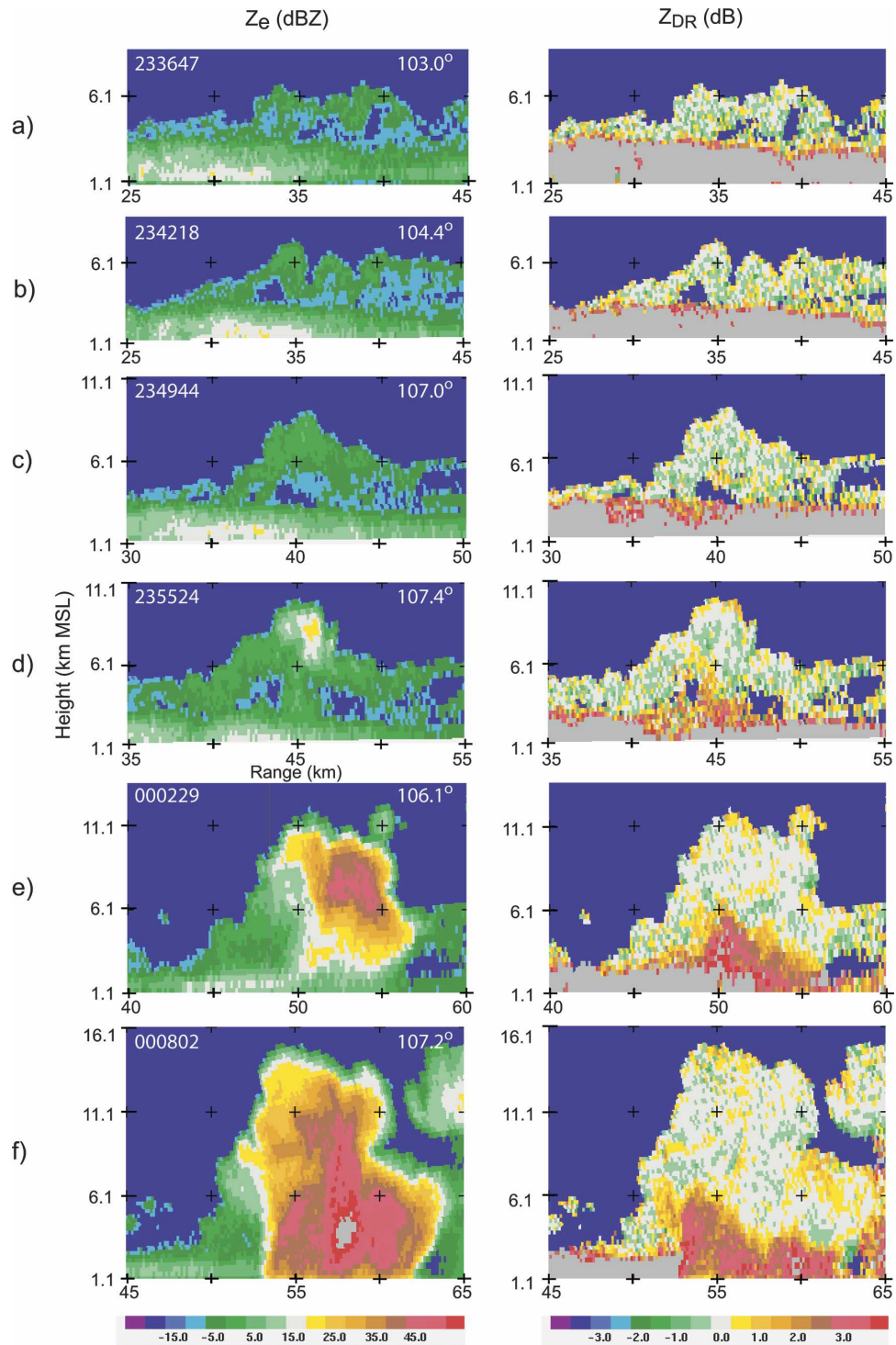


FIG. 3. Central RHIs through the developing cell of 29 June: (a)–(f) six successive sweeps, displaying (left) Z_e , and Z_{DR} , and (right) radial velocity (VEL) and LDR. Radial velocity is positive away from the radar. Azimuth angles are noted, selected to show best the development of Z_{DR} . The altitudes are in 5-km increments above ground, labeled as above MSL. Range from the radar varies, keeping the cell in the center of the frame. The prominent gray areas in the Z_{DR} plots show values above 4.25 dB, attributed to insects. LDR is thresholded at 119 dB on the cross-polar received power. In (e), the data below about 2 km MSL (LDR especially) are contaminated by a second-trip echo, and the high LDR at the cloud top is a sidelobe effect. The text emphasizes the positive Z_{DR} at 40-km range in (c), just below 6.1 km MSL, and the later, more positive Z_{DR} that extends higher.

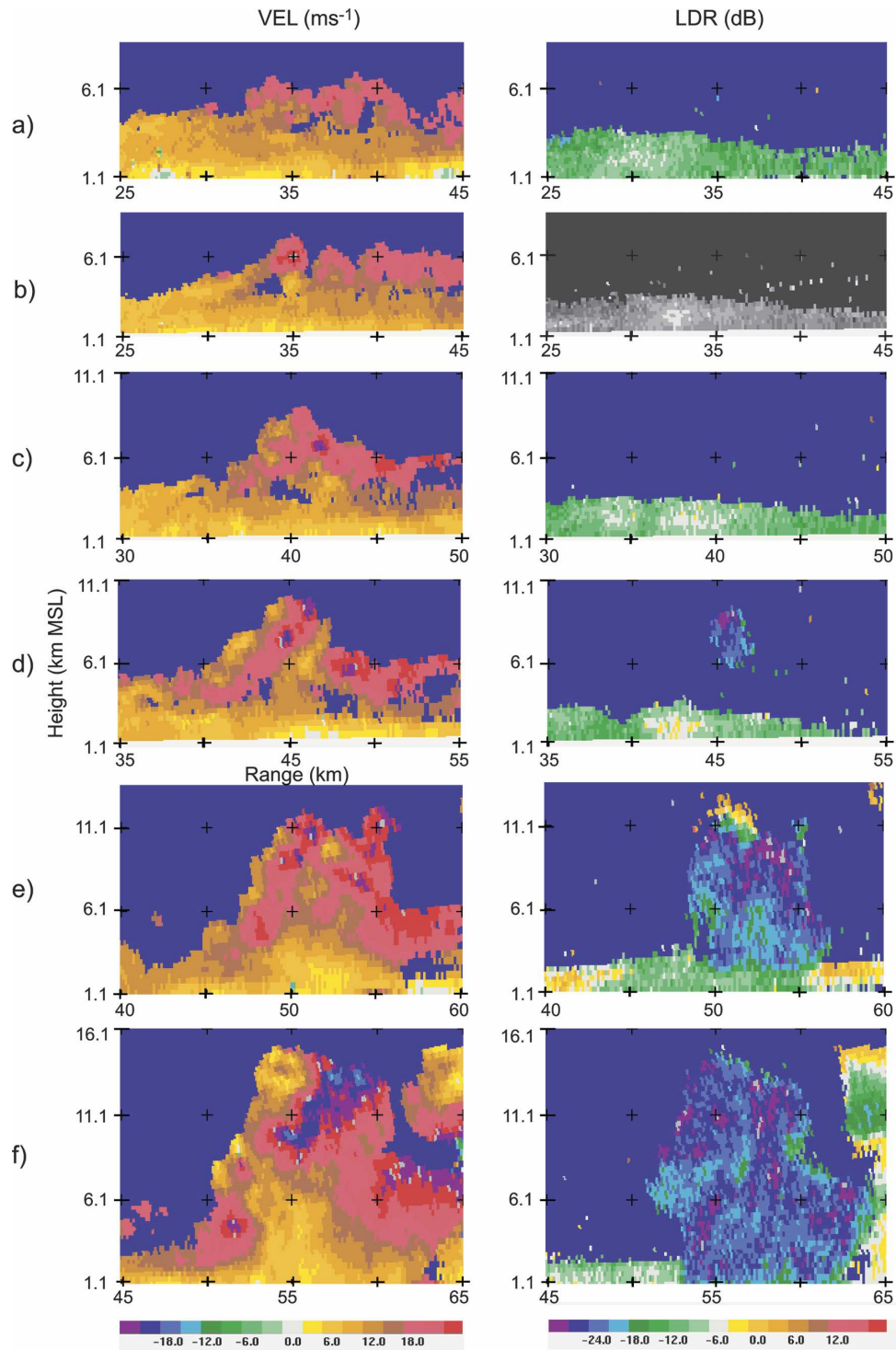


FIG. 3. (Continued)

The PPIs in this case show that the distinctive radar signature of the insect-filled layer is completely separate from the developing radar echo of the cloud, above it. The evidence is not presented for this case, but simi-

lar evidence is given below (in Fig. 7) for the 23 June case.

The specific convective element of interest on 29 June is first seen in Fig. 3b. It grew within a small region

of convective elements seen in Fig. 3a, at which time the echo tops were at about 6.9 km MSL (about -15°C), but individual elements cannot be tracked backward in time before 2342 UTC (Fig. 3b). The earliest data on the convection were at 2330 UTC, at which time the highest echo top was at about -10°C . The radar echo from the clouds in Figs. 3a and 3b (with maximum Z_e between -2.5 and $+2.5$ dBZ) is certainly Bragg scattering. It probably is mostly so in Fig. 3c as well, except perhaps for a small spot of 5 dBZ that may be the very first sign of echo from hydrometeors. The conventional first echo is evident in Fig. 3d, at about 20 dBZ (yellow), and it then intensifies rapidly while expanding upward, downward, and sideways.

The cloud was 15 km west of the main storm at the time of Fig. 3b. It moved eastward at about 13 m s^{-1} and its radar echo is just starting to mingle with that of the main storm at the time of Fig. 3f.

One noteworthy feature of the cloud echo in its earliest stages is the striking weak echo region at the base of the growing turret, seen in Figs. 3b and 3c. The base of this weak echo region is at the top of the insect echo, at about 3.5 km MSL, above the cloud base for the main storm [the lifting condensation level (LCL)], which was calculated to be 3.1 km MSL. The top of the weak echo region in Fig. 3b is at 5 km MSL, so much or all of it is certainly within cloud, where it presumably represents an unmixed updraft core, with little or no Bragg scattering and very few of the insects from the boundary layer. (Note that the radial convergence associated with the weak echo region, in the velocity panel of Fig. 3b, does not extend down into the insect layer.) Weak echo features much like this, similarly situated, were found to be common in the very early stages of small cumulus in Florida (Knight and Miller 1998).

The first precipitation echo that would be identified as such using Z_e alone is in Fig. 3d, but the first Z_{DR} signal identified as from water drops within cloud is in Fig. 3c, just at the top of the weak echo region at 40-km range, 5.5 min earlier. This region of positive Z_{DR} extends to about 6-km MSL, but since Z_e is increasing upward at its location, the top of the water drop population that presumably generates it could be higher. Its Z_{DR} could be masked by echo with zero Z_{DR} from the Bragg scattering. (We have never seen significantly nonzero Z_{DR} from echoes that appear to be Bragg scattering.)

The top of the positive Z_{DR} has risen to about 7 km MSL in Fig. 3d, and the positive Z_{DR} now corresponds with what appears to be a vertical precipitation shaft, in the Z_e panel of Fig. 3d, that extends down through the center of the weak echo region. This is directly beneath

the stronger echo above (20 dBZ at 8.5 km MSL) that is composed of ice because of its low temperature and zero Z_{DR} . The weak precipitation shaft, with maximum Z_e of 5 dBZ, contains raindrops some of which must be considerably larger than 1 mm in diameter in order to produce the observed Z_{DR} values of 1.5 to 2 dB up to a height of 5 km MSL. [See, e.g., Table 1 in Knight et al. (2002). Drops that are 1 mm in diameter produce Z_{DR} of about 0.2 dB; 2 mm, about 0.7 dB.] Finally, in Figs. 3e and 3f, there is a massive column of strongly positive Z_{DR} , which is associated in Fig. 3f with values of Z_e up to 45 dBZ.

These regions of positive Z_{DR} correlate well with the locations of convergence in the radial velocity field, especially in Figs. 3c and 3d. The overall evidence is strong that they arise from drops within the updraft, within and below cloud.

It is quite remarkable that such large raindrops occur first so early in the echo history of this cloud: in a manner completely distinct from what would conventionally be called the first precipitation echo. The conventional first echo forms near cloud top, intensifies rapidly and descends to the ground (Figs. 3d–f), while the raindrop Z_{DR} forms low and intensifies its Z_{DR} significantly, but its reflectivity factor does not increase a great deal until much later. Its location does not coincide with the reflectivity maximum of the cloud. Early, it correlates best with a local minimum in Z_e , while later it is always upwind of the region of maximum Z_e . This is best shown in plan view, and one example is given in Fig. 4, traced from a PPI. This underscores the fact that the combined Z_e and Z_{DR} time–height diagrams in this paper are not to be taken to imply that the maximum values of Z_e and Z_{DR} coincide: in fact they virtually never coincide except in rain well below the melting level. Sometimes the Z_{DR} maximum does correspond with a weak, local maximum in Z_e (as shown in Fig. 8, below).

The regions of the positive Z_{DR} interpreted as indicating raindrops finally attain 4 dB within the cloud in Fig. 4e, and come to correspond with Z_e values up to 40 dBZ (within cloud; higher within precipitation near the ground), in Fig. 4f. Note that much of the structure of Z_e , Z_{DR} , and the radial velocity (VEL) in Figs. 4e and 4f is consistent with the updraft being on the left and precipitation, presumably accompanied by downdraft, on the right, with a separation a little to the right of 50-km range in Fig. 3e, and to the right of 55 km in Fig. 3f. Two lobes of positive Z_{DR} rise to about 7 km MSL to the left of 55-km range in Fig. 3f, and could very well be supercooled raindrops recycled in the updraft, coming from melted ice.

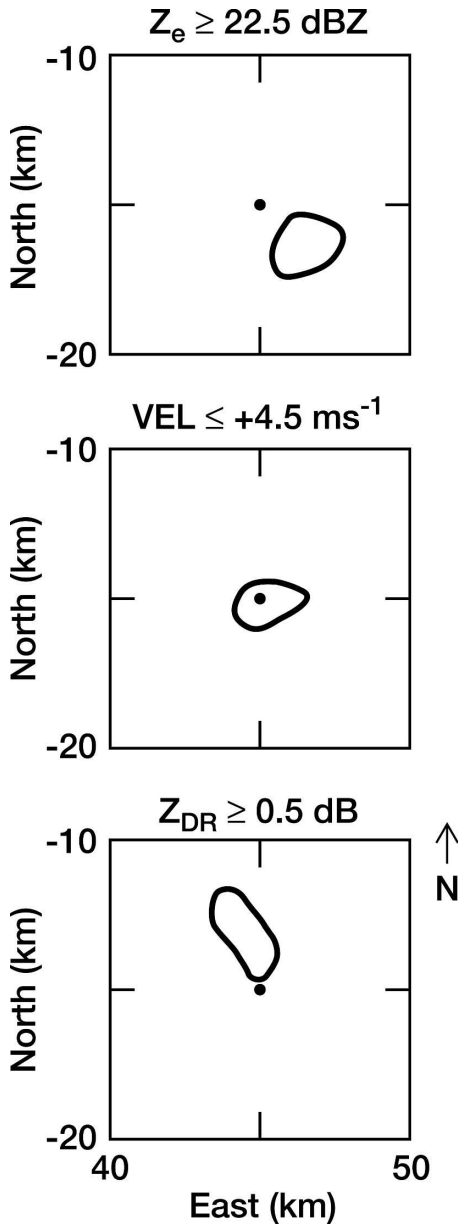


FIG. 4. Tracings of contours defining maximum values of (top) Z_e and (bottom) Z_{DR} , and (middle) minimum VEL from the 29 June case, the 5.4° elevation angle sweep at 2358:00. Altitude at center, 45 km east and 15 km south of S-Pol, is 5.6 km MSL. The environmental radial velocity at that height is 18–20 m s^{-1} . Lower values prevail at lower altitudes, so the minimum is taken as an indicator of the strongest updraft. This relationship, with positive Z_{DR} upwind and maximum Z_e downwind of the updraft, is seen also in Fig. 8, and is an obvious feature in the PPIs here, though it is not obvious in RHIs in Fig. 3.

b. 23 June

The sounding for this case is presented in Fig. 5. It has a CAPE of only 204 J kg^{-1} . As in the 29 June case, the Z_{DR} history is the main interest, and the combina-

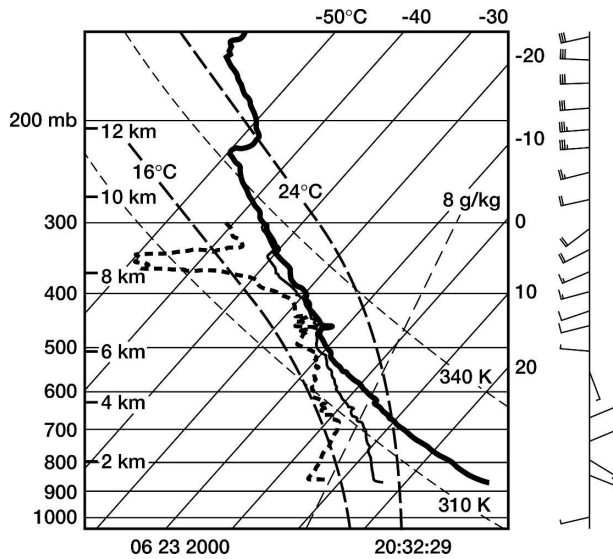


FIG. 5. Sounding for the 23 June case. As in Fig. 2, except the two pseudoadiabats shown have no special significance.

tion Z_e and Z_{DR} time–height diagram is Fig. 6. As in the previous case, the first Z_{DR} precedes or is about simultaneous with a conventional, first precipitation echo near cloud top.

Figures 7 and 8 show examples of Z_e and Z_{DR} from the 2121–25 volume scan and of Z_e , Z_{DR} , and radial velocity from the 2127–31 volume scan. Figure 7 shows six consecutive sweeps from the volume scan in which the Z_{DR} identified as water drops first appears. Figure 7a (1.6° elevation, center of frame about 2.2 km MSL) shows the radar thin line, with up to 10 dBZ along with Z_{DR} consistently above 4.25 dB, the upper level on the color table. Figure 7b (2.9 km MSL center of frame) skims the top of it. Figure 7c (3.7 km MSL) shows a ring

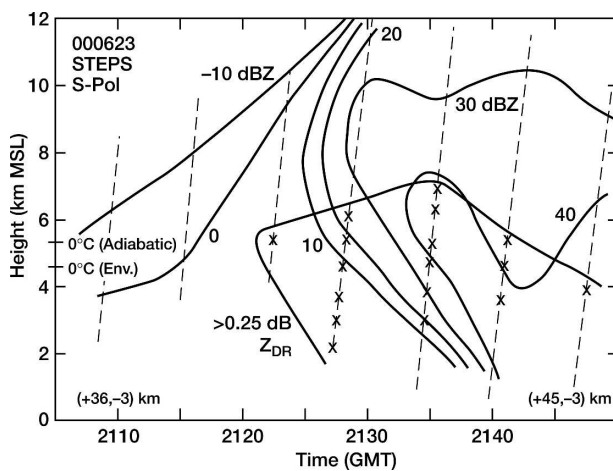


FIG. 6. Time–height diagram, for the 23 June case, like Fig. 2.

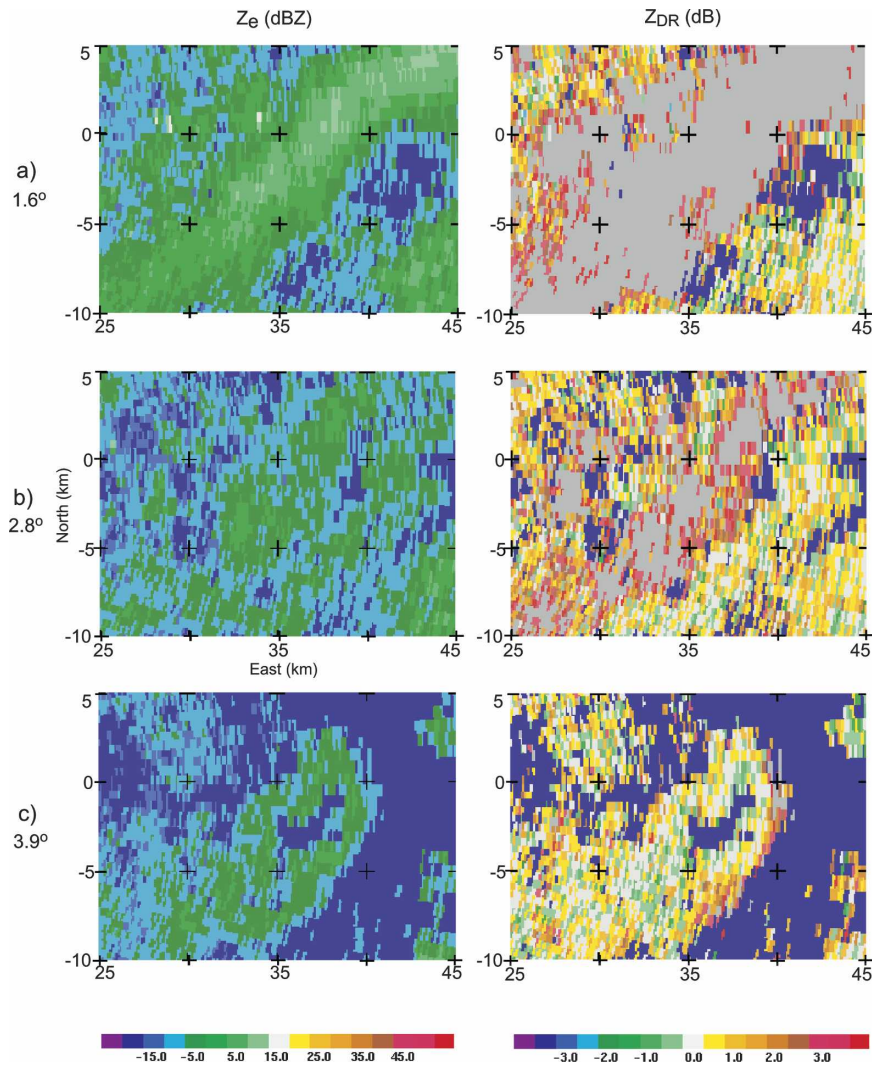


FIG. 7. (a)–(f) For the 23 June case, detail of six consecutive PPI sweeps of Z_e and Z_{DR} , starting at 2121. Heights of the frame centers are approximately 2.2, 2.9, 3.7, 4.5, 5.2, and 5.9 km MSL, respectively. Note the “insect convergence” (the radar thin line, oriented southwest–northeast) in (a), with its top just grazed in (b). Echo specifically related to the study cloud appears first in the center of (c), with a ring of Bragg echo surrounding a weak-echo region. In this volume scan, the first detectable positive Z_{DR} signal appears in (e) only.

of echo at -5 to 0 dBZ surrounding a weak echo region in the center of the frame. This is approximately at the estimated cloud base, and is interpreted as Bragg scattering. In Fig. 7c the value of Z_{DR} within the area of reflectivity related to the cloud averages approximately zero and Z_e is low, so there is no evidence of transfer of the very high Z_{DR} insects from the thin line up into the cloud. (There is no LDR signal here because the cross-polar component is below the noise level, but that implies that LDR is much lower than that in the insect layer.)

Figures 7d–f are the next three levels (respectively at 4.5 km, which is about the freezing level; 5.2 km; and 5.9 km MSL), and reveal the first, definitely significant

patch of positive Z_{DR} at 5.2 km, just west of the cross marking 0° , 40°E in the 6.2° scan, Fig. 7e. It is significant because of its continuity with the Z_{DR} signal shown in Fig. 8b, which is at the same level as Fig. 7e. Note also the small patch of Z_e about 5 dBZ at the southeast corner of the cloud echo in Fig. 7e. This, along with a similar patch in Fig. 7f above it, may be the first weak, conventional indication of precipitation in the reflectivity, since they also show continuity, and very considerable intensification, in Figs. 8b and 8c.

Figure 8 shows the rapid intensification and spread of Z_e from hydrometeors in the eastern part of the cloud, as well as intensification of Z_{DR} in the patch of positive

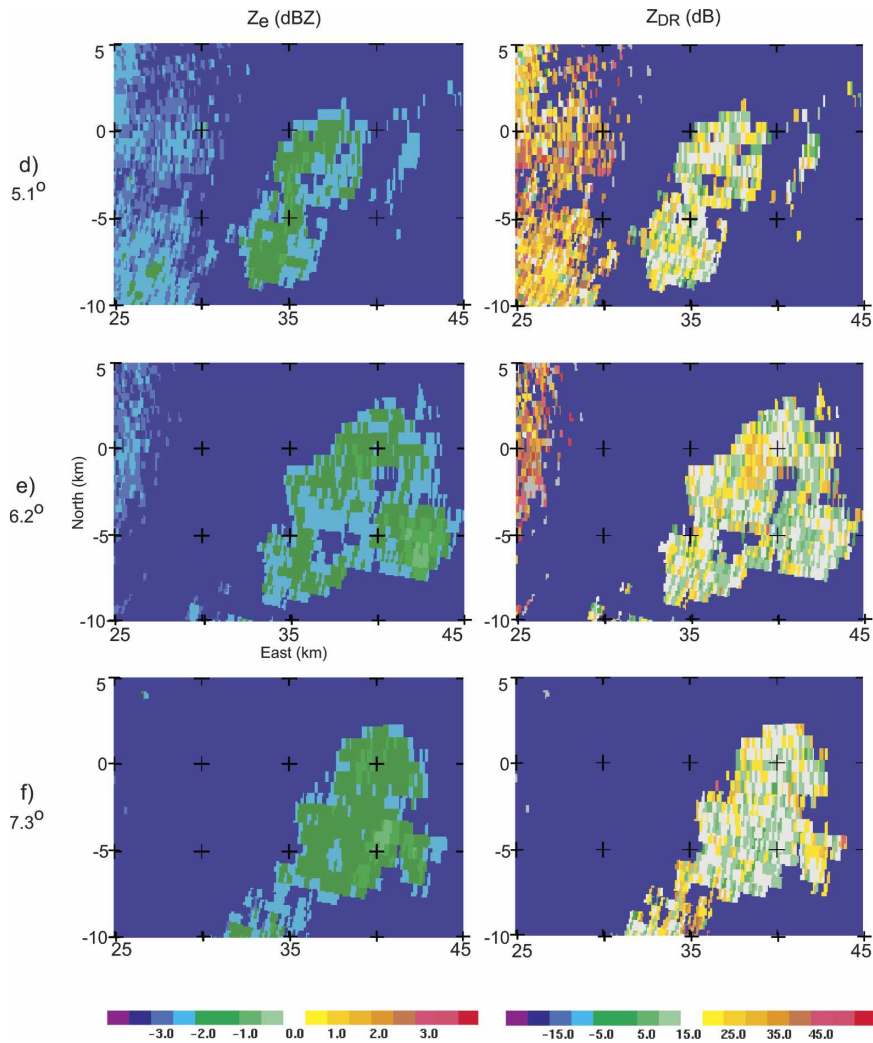


FIG. 7. (Continued)

Z_{DR} to the west and its spread both upward and downward. Figure 8 also shows the corresponding radial velocity field, the east–west component of the wind since the radar is due west. As was seen in the previous case (Fig. 4), if radial velocities typical of lower levels correspond with updraft, the positive Z_{DR} is at the western edge of the updraft and the maximum Z_e is toward the east, which is downwind with respect to the environmental winds at that level. The Z_e values associated with the positive Z_{DR} are only up to about 5 dBZ at the most, but they do form a slight, local maximum.

It is somewhat puzzling that looking at Z_e and Z_{DR} alone, one might identify two fairly distinct turrets in this cloud. The eastern one has the intensifying Z_e (at the stage of Figs. 7 and 8) and the western one the big water drops. However, the radial velocity data show them very clearly as a single dynamic entity.

The first appearance of positive Z_e just above the

freezing level raises the possibility of its originating as needle crystals, falling with their long axes horizontal. While the data are not sufficient to reject this origin with absolute certainty, it seems most unlikely from any standpoint in a vigorous convective turret. It would require either a surprisingly high concentration of ice nuclei active at or above -5°C or a vigorous Hallett–Mossop process that produces enough needles that they dominate the radar echo that would arise from the graupel that are needed to produce them. If needle crystals were involved, it would be surprising to see the positive Z_{DR} cross the 0°C level with little disturbance.

c. 4 July

The only local sounding on this day, at 1730, showed virtually no CAPE (Fig. 9), but several rather weak cumulus developed about 6 h later more than 50 km to the east. They moved east-northeast, with new turrets

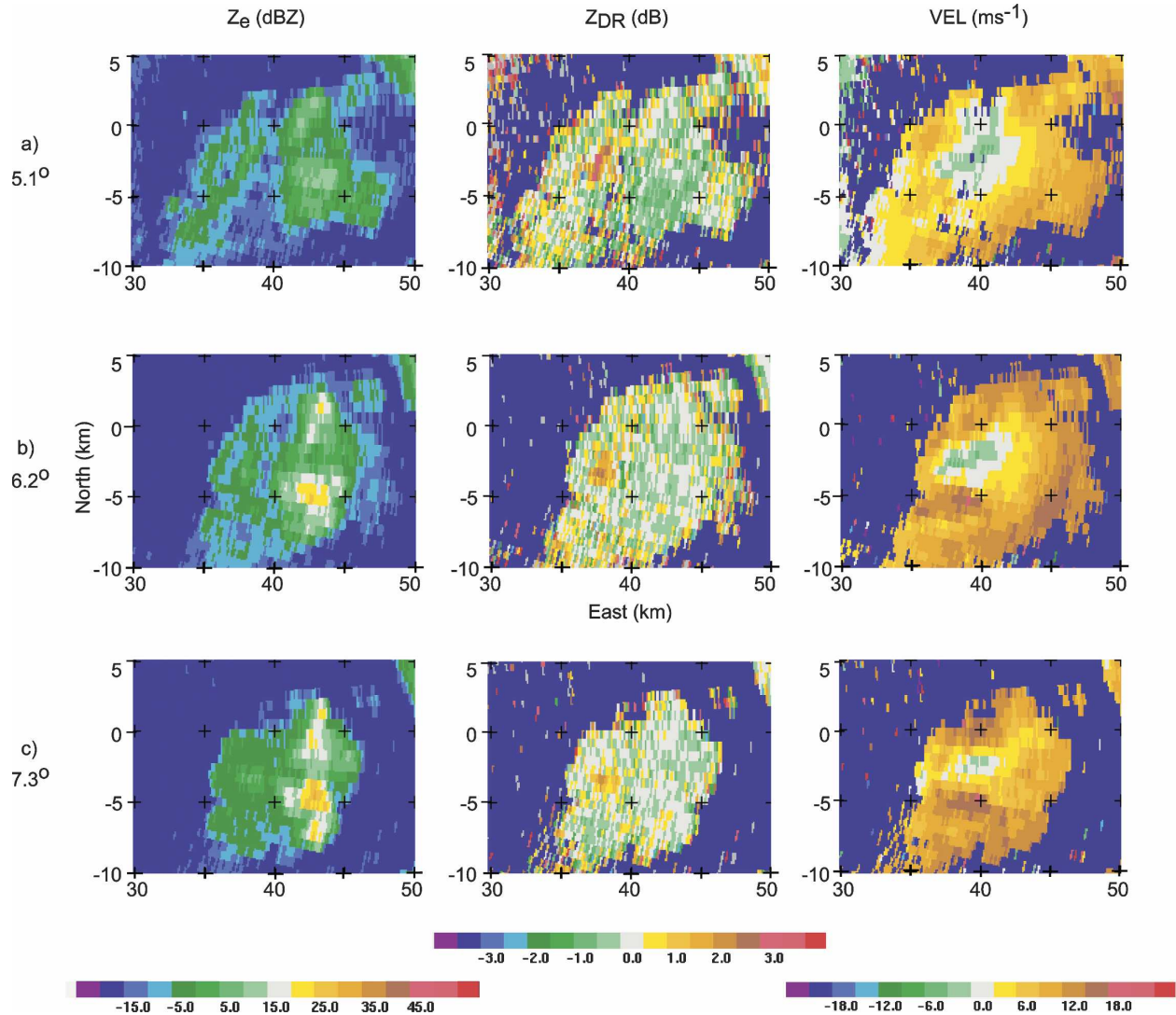


FIG. 8. (a)–(c) For the 23 June case, detail of three consecutive PPIs of Z_e , Z_{DR} , and VEL, from the volume scan 6 min after that in Fig. 7. Note particularly the vertical growth and the intensification of the positive Z_{DR} signal at about (38, -3) km, and the relations between the locations of the positive Z_{DR} values, the updraft (the conspicuous minimum in VEL), and the conventional “first echo,” now much stronger than in Fig. 7.

on their west sides, and most of them had positive Z_{DR} columns on their western sides, similar to those in the first two cases.

Figure 10 is the time–height diagram for Z_e and Z_{DR} of one of the cells. Again there are very early, positive Z_{DR} values rising well above the freezing level as the traditional first precipitation echo develops. Figure 11 is from a single series of RHIs that was made at about the time of maximum echo height, showing the positive Z_{DR} column at the upwind edge.

d. 5 July

The storm of interest on 5 July started very close to S-POL, and was not recognized there, so S-Pol did not

scan it in its early stages. It was scanned by CHILL, and good data were acquired even though the range was more than 70 km. The surface data show a strong moisture gradient in the area, and a nearby sounding was altered accordingly in its low levels, giving the sounding in Fig. 12. The CAPE was very roughly 1000 J kg^{-1} , either more or less depending upon the assumed value of surface moisture. The time–height diagram is given in Fig. 13.

The early echo behavior of this cloud was similar in some ways to the previous three, but very different from them in others. It too grew above a low-level accumulation of insects, as identified by very high Z_{DR} , Z_e around 15 dBZ, and high LDR; it had at least 10 min

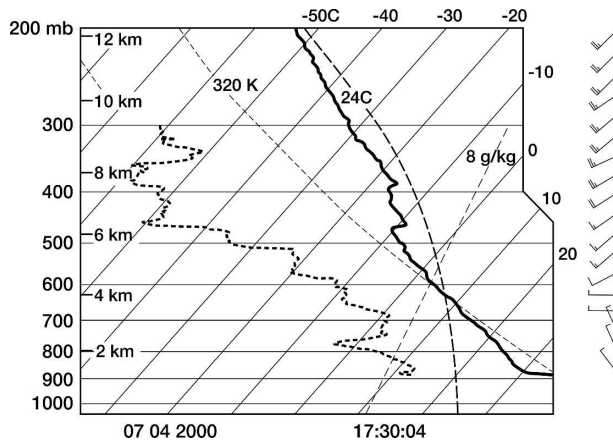


FIG. 9. Sounding for the 4 July case.

with cloud tops well above the 0°C level before its first precipitation echo appeared; and it developed an obviously significant volume of positive Z_{DR} extending above the freezing level early in its history. However, one major difference from the other cases is that its conventional, first precipitation echo preceded the positive Z_{DR} , and it looks as if there was an initial, relatively weak and brief updraft pulse that evolved into the stronger one. As in the other three cases, the positive Z_{DR} was west of the area of maximum Z_e , and this case provides an especially nice example of the positive Z_{DR} well above the freezing level correlating well with a strong perturbation in the field of radial velocity, which very probably correlates in turn with updraft (Fig. 14). Figure 14 also shows the strong, local, cyclonic circulation at a lower level, which lasted from about 2245 to 2300, a feature seen only in this case.

3. Discussion

This paper reports the first observations of a consistent dynamic context in which water drops with diameters more than one millimeter are seen very early in developing cumulus clouds. It is also the first in which the clouds are known to have continental cloud droplet populations, which tends to inhibit the direct formation of large liquid drops. Previous observations of early, positive Z_{DR} in cumulus were by Caylor and Illingworth (1987) in England, Illingworth (1988) and Tuttle et al. (1989) in Alabama, and Knight et al. (2002) in Florida, in all of which the clouds may have been relatively maritime. The radar data in the first two papers were not very detailed, and there was no information in any of them on either the CCN or the cloud droplet populations. The South Dakota School of Mines and Technology armored T-28 aircraft flew in STEPS, and

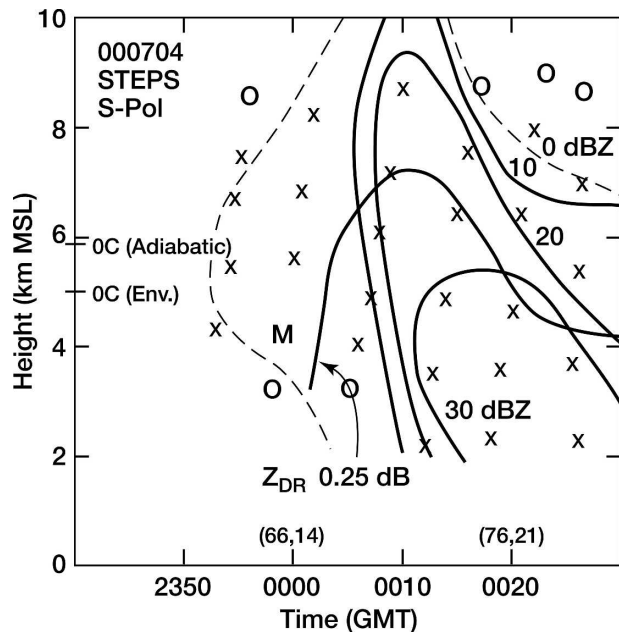


FIG. 10. Time–height diagram of Z_e , with envelope of significantly positive Z_{DR} indicated, for the 4 July case. Here the \times symbols indicate all the data points, not necessarily significantly nonzero Z_{DR} values as in the other time–height diagrams. The “O” symbols indicate locations with data but no echo identified with the cloud, and “M” is a missing sweep.

its forward scattering spectrometer probe (FSSP) routinely registered maximum cloud droplet concentrations in the range of 800–1000 cm^{-3} in cumulus penetrations (A. Detwiler 2002, personal communication). Its flights included 23 and 29 June, but not 4 or 5 July.

The two main questions raised by the observations here are the origin of the water drops responsible for the very early, positive Z_{DR} values, and their significance for precipitation development within the cloud. It was a surprise to find these, and they are likely to indicate something important, but the assessment of that will require more detailed attention to the very early stages of cumulus clouds than has been usual in the past. Finally, at a more general level, we give a brief discussion of the use of radar in support of field programs aimed at understanding the formation of precipitation in cumulus.

a. Origin of the big drops

In all of these cases the convection formed initially in association with a surface convergence that caused a high concentration of insects, visible on radar (Wilson et al. 1994). However, there is no indication of the insects rising into the clouds in their early echo stages. In

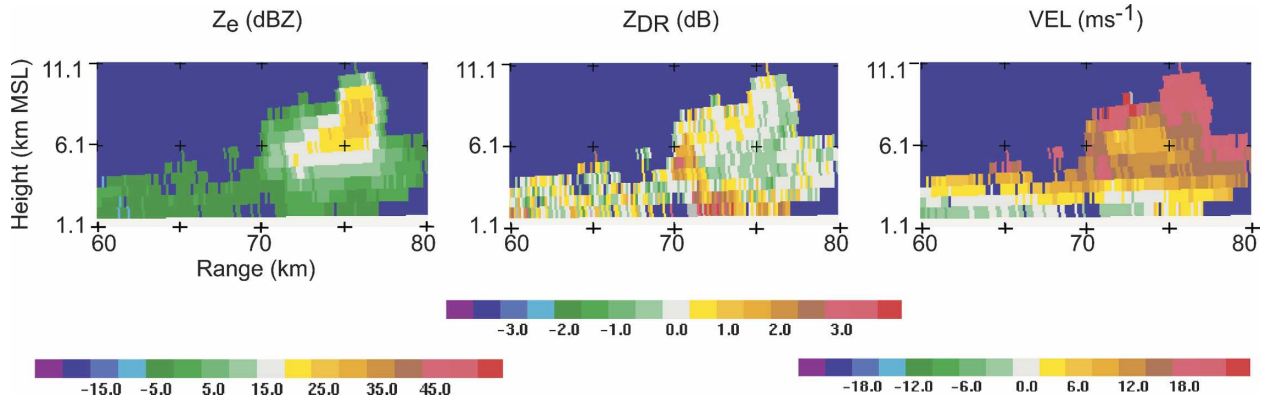


FIG. 11. RHIs of Z_e , Z_{DR} , and VEL from the 4 July case, the 75° azimuth scan at 0011:11 on 5 July. Note the positive Z_{DR} extending above 6 km MSL on the upwind, western side of the echo.

fact, as illustrated in Figs. 3a–c, the top of the insect layer is often strikingly flat, even with fairly vigorous convection above it, and there is no indication in the radial velocity fields of vigorous updrafts within the insect layer. The radar data allow more possibility for insects being carried up into the cloud later, when the updrafts are probably stronger, with roots closer to the ground. Nevertheless, coalescence on ultragrant nuclei is one possibility for the origin of the big drops, and there is no way to rule out small insects as ultragrant nuclei.

Earlier work referred to above ascribed positive Z_{DR} values early in cumulus to drops grown initially by a coalescence process. Tuttle et al. (1989) traced the positive Z_{DR} they observed back to small cumulus in which coalescence was clearly producing raindrops that were then elevated in a stronger updraft, into a bigger, deepening cloud. The clouds observed here also can be traced back to much smaller cumulus, but these do not

show a positive Z_{DR} signal or any other indications of precipitation in the radar data.

The possible origins of the big drops are the usual ones: coalescence with or without ultragrant nuclei (e.g., Johnson 1982), or the coalescence growth of drizzle drops that might be recycled, melted ice. It is noteworthy that the regions of positive Z_{DR} are not only present very early, but continue to be present well into the stage of precipitation reaching the ground. In these later stages, they may be explained most readily by the recycling mechanism suggested in a similar case in Colorado by Tuttle (1993): the sheared cloud precipitates graupel downwind, but the updraft overrides the precipitation and ingests some of it from beneath the melting level. In the cases presented as Figs. 2, 6, and 10, the fact that the first positive Z_{DR} may slightly precede the early, conventional precipitation echo adds some doubt to this interpretation, but does not rule it out. The same recycling mechanism might be occurring,

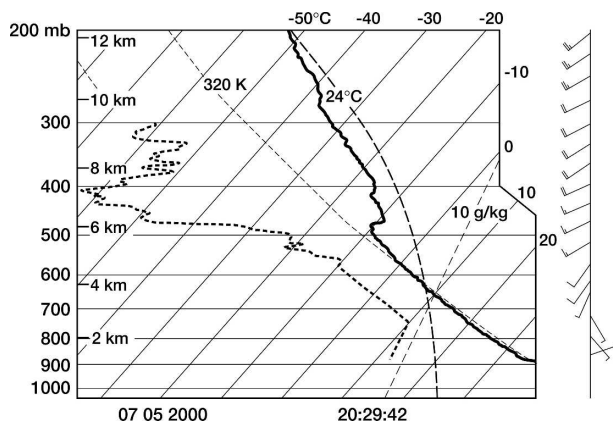


FIG. 12. Sounding for the 5 July case, at the time indicated but with the lower-level moisture adjusted according to a strong surface moisture gradient on that day.

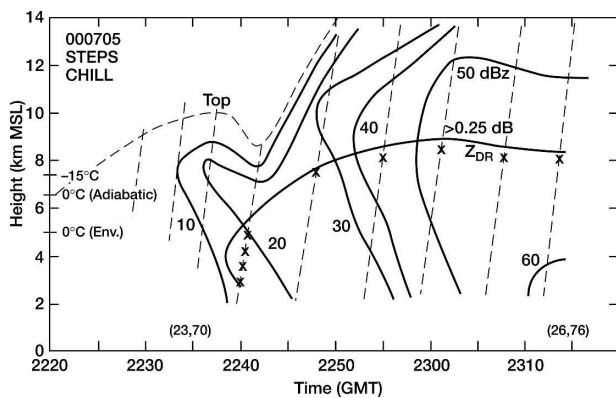


FIG. 13. Time–height diagram of Z_e for the 5 July case, with locations of significantly positive Z_{DR} values indicated, as for Figs. 2 and 6.

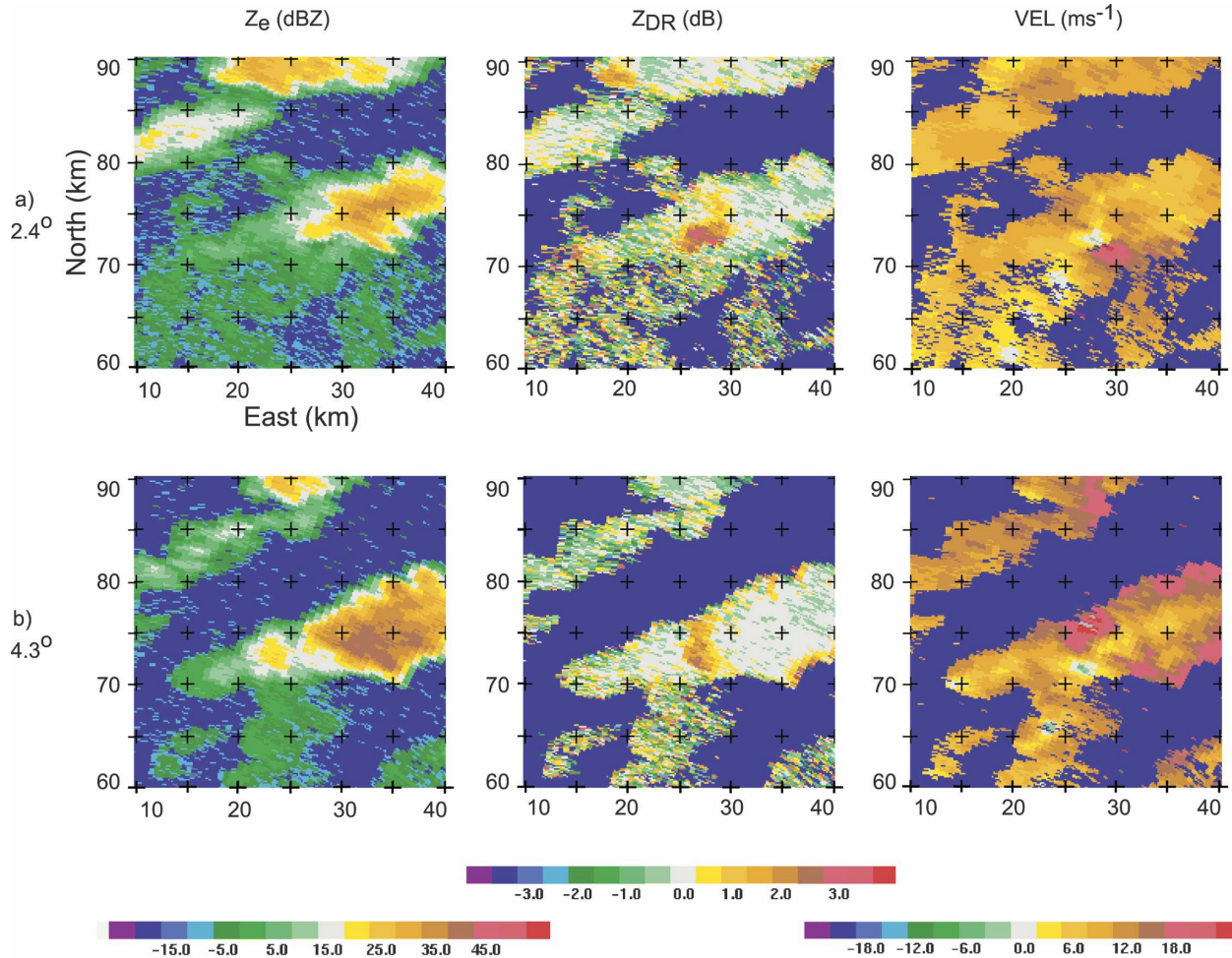


FIG. 14. PPIs of Z_e , Z_{DR} , and VEL for the 5 July case: (a) at 2254:03, center of frame 3.3 km MSL; and (b) at 2255:08, 5.9 km MSL. The prominent patch of strongly positive Z_{DR} near the center of the frame is clearly related to the strong, radial velocity perturbations in the cloud.

but at hydrometeor concentrations and sizes below radar detectability.

The author tends to favor the recycling mechanism, largely because it appears to be more likely in the later, more mature stages of the clouds. See Fig. 3f and its discussion above. That makes a simpler story: the same mechanism can be appealed to throughout. However, that is not a very strong argument, and there is not enough information rule out any of the possible origins of the drops responsible for the early, positive Z_{DR} values. (While the poor time resolution makes estimates quite rough, it appears that all cases may have at least about 10 min between the time the cloud top passes the -10°C level in the environment and the first appearance of the positive Z_{DR} . That may be enough time for the recycling to occur, and the case in Fig. 3 may have 20 min or more.) Full-fledged growth trajectory studies would be needed to establish the plausibil-

ity of any hypothetical origin. Such studies require realistic fields of both wind and liquid water content, and probably the best hope for that, for the early stages of cumulus, comes through modeling. The priority would be to get the onset of the convection dynamically realistic and verified as much as possible by observation, which in turn makes it critical in future work to obtain data extending back to the earliest stages of individual clouds.

b. Significance of the big drops

Do these big drops make a difference? Those that produce the earliest, positive Z_{DR} values do not appear to contribute directly to the conventional first precipitation echo. However, being in and toward the upwind side of the updraft, they might act to spread ice throughout the clouds at fairly early times through drop shattering upon freezing, which could be an important

source of ice for drops this large (e.g., Knight and Knight 1974). Another potential contribution to creating more ice would be through the Hallett–Mossop process: by freezing and then riming. Perhaps the greatest potential importance of the finding of big drops very early in these clouds, however, is indirect: not from the drops themselves, but from what they might signify. The detectable, positive Z_{DR} regions illustrated above represent (very roughly) water drops of 1 mm diameter and larger in concentrations less than 1 m^{-3} , and the greater significance may be that this probably implies considerably higher concentrations of drops in the few-hundred-micron-diameter range both at the same and at earlier times. This might extend 5 or even 10 min before the first detectable echo from ice, not producing a detectable Z_{DR} signature, and could be much more important in terms of the cloud development than the smaller concentrations of larger drops that give rise to the observed, positive Z_{DR} .

Since three of the four cases observed in STEPS had water drops very early, this may be a rather common feature in vigorously developing, continental cumulus. In the exceptional case, in which the positive Z_{DR} column first appeared well after the first echo from growing ice hydrometeors (5 July, Fig. 13), the main convective impulse evidently included a smaller cumulus in which the ice process was already active.

c. *The radar scanning procedures*

We have argued that time is a critical factor for a study aimed at understanding the early formation of precipitation in cumulus. Generally speaking, calculations of how fast hydrometeors grow in different environments are probably much more reliable than knowledge of the environments cumulus clouds provide and how long they last. This is not for lack of aircraft data within clouds, of which there has been a great deal. It is mostly from not knowing the overall cloud history and especially, for the early formation of precipitation, the very early cloud history.

Direct observations will probably never be complete enough to provide direct understanding of how precipitation forms in cumulus, since interpretations from remote sensing are too ambiguous and aircraft are too limited in their coverage. Numerical modeling is the only approach, and radar appears to be the only way to obtain information for both initializing and verifying models of cumulus initiation. The earliest stages appear to be critical for understanding the microphysical evolution. For instance, what could be more important for understanding ice initiation in cumulus than the temperature history of cloud top? While radar is the obvi-

ous way of getting this kind of information, it turns out to be deceptively difficult in practice, and so we devote a few words to it here.

The problem, of course, is that one wants detailed data from very early, and yet one doesn't know very early which of (usually) many small cumulus will develop further and become good cases. Radars cannot scan fast enough to get detailed data everywhere. The main piece of advice is that it is very difficult to resist "chasing" good-looking cumulus with the radar, but that is a temptation that must be resisted. If a cumulus looks promising, it is already too late, usually much too late. The main lesson the author learned from STEPS, in this regard, was that although one would like high-resolution data, it is far more valuable to have early, low-resolution data than none at all. Unless the initiation is much more predictable than it was in STEPS (e.g., as it might be in the vicinity of an isolated mountain) the strategy for capturing the early stages should be to settle for the lowest resolution that is still barely tolerable, cover a big sector, and only narrow in on a cloud when one is quite sure that it is going strong and that the early radar data have been obtained. The lesson for me was that my standards for barely tolerable before STEPS were considerably higher than they are now. The 6-min time resolution represented by Fig. 3 is still very useful, even in the early stages.

The specific advice is to use routine, wide-sector PPI volume scans almost all the time. RHIs entail (for S-Pol) slower scan rates, more reversals of antenna direction, and a smaller sector of coverage for a given time between volume scans. It is also more difficult to comprehend overall cloud evolution in real time when the radar is in RHI mode. RHIs can be used in brief interruptions of the routine scanning, taking one or two minutes to get a narrow sector of vertical slices in a very good case. While every situation is different, going back to the STEPS area with the same radar, devoted to early echo studies, I would suggest something along the following lines: a routine PPI sector of 180° , with volume scans every 5 min, scan rate 10° s^{-1} , and 15 elevation steps from 0.5° to 20° . This would use 64-pulse averaging, to give an azimuthal resolution of about 1° . Such a procedure would have provided much more first-echo data from STEPS. However, one of the observations gained from going through the whole dataset looking for first echoes was an appreciation that convective systems fairly often contained no distinguishable first echoes at all. These consisted of cellular convection, but with no isolated, new radar echoes. In these, the primary mechanisms of precipitation formation may have little importance.

Acknowledgments. The radar data were collected through the efforts of the personnel supporting and operating the S-Pol and CHILL radars, and I thank especially Bob Rilling and Jay Miller for invaluable assistance in accessing the data. I thank L. J. Miller for very thoughtful and helpful comments and suggestions on this manuscript.

REFERENCES

- Caylor, I. J., and A. J. Illingworth, 1987: Radar observations and modeling of warm rain initiation. *Quart. J. Roy. Meteor. Soc.*, **113**, 1171–1191.
- Cooper, W. A., and R. P. Lawson, 1984: Physical interpretation of results from the HIPLEX-1 experiment. *J. Climate Appl. Meteor.*, **23**, 523–540.
- Illingworth, A. J., 1988: The formation of rain in convective clouds. *Nature*, **336**, 754–756.
- Johnson, D. B., 1982: The role of giant and ultragiant aerosol particles in warm rain initiation. *J. Atmos. Sci.*, **39**, 448–460.
- Knight, C. A., and N. C. Knight, 1974: Drop freezing in clouds. *J. Atmos. Sci.*, **31**, 1174–1176.
- , and L. J. Miller, 1998: Early radar echoes from small, warm cumulus: Bragg and hydrometeor scattering. *J. Atmos. Sci.*, **55**, 2974–2992.
- , J. Vivekanandan, and S. G. Lasher-Trapp, 2002: First radar echoes and the early ZDR history of Florida cumulus. *J. Atmos. Sci.*, **59**, 1454–1472.
- Lang, T. J., and Coauthors, 2004: The severe thunderstorm electrification and precipitation study. *Bull. Amer. Meteor. Soc.*, **85**, 1107–1125.
- Tessendorf, S. A., L. J. Miller, K. C. Wiens, and S. A. Rutledge, 2005: The 29 June 2000 supercell observed during STEPS. Part I: Kinematics and microphysics. *J. Atmos. Sci.*, **62**, 4127–4150.
- Tuttle, J. D., 1993: Multiparameter radar observations of developing turrets in a High Plains storm. Preprints, *26th Int. Conf. on Radar Meteorology*, Norman, OK, Amer. Meteor. Soc., 516–518.
- , V. N. Bringi, H. D. Orville, and F. J. Kopp, 1989: Multiparameter radar study of a microburst: Comparison with model results. *J. Atmos. Sci.*, **46**, 601–620.
- Vivekanandan, J., D. S. Zrnic, S. M. Ellis, R. Oye, A. V. Ryzhkov, and J. Straka, 1999: Cloud microphysics retrieval using S-band dual-polarization radar measurements. *Bull. Amer. Meteor. Soc.*, **80**, 381–388.
- Wilson, J. W., and W. E. Schreiber, 1986: Initiation of convective storms at radar-observed boundary-layer convergence lines. *Mon. Wea. Rev.*, **114**, 2516–2536.
- , T. M. Weckwerth, J. Vivekanandan, R. M. Wakimoto, and R. W. Russell, 1994: Boundary layer clear-air radar echoes: Origin of echoes and accuracy of derived winds. *J. Atmos. Oceanic Technol.*, **11**, 1184–1206.